

# Multi-Electrode Electroretinography with Transparent Microelectrodes Printed on a Soft and Wet Contact Lens

Lunjie Hu, Saman Azhari, Qianyu Li, Hanzhe Zhang, Atsushige Ashimori, Kazuhiro Kimura, and Takeo Miyake\*

Visual electrophysiology measurements are crucial in ophthalmology as they are frequently used for diagnosing and treating numerous ocular diseases. Therefore, optically transparent and flexible electrodes with high sensitivity at localized regions are in high demand. Here, it is aimed to develop a soft, transparent, multi-electrode system assembled on commercially available soft contact lenses and assess its application in measuring Electroretinography (ERG) responses in rabbits. A biocompatible multi-electrode system on commercial disposable soft contact lenses is successfully constructed, showing 95% cell viability, 82% optical transparency over the visible range, and good flexibility at 10% strain. Direct current (DC) voltage is used to produce a highly resistive overoxidized poly(3,4-ethylenedioxythiophene) (PEDOT) layer that covers all parts of the electrodes except the sensing region, which, owing to its high conductivity, can accurately measure electrical signals from local regions of the cornea. Spatially resolved ERG recordings of rabbits are obtained with superior signal quality using this multi-electrode system. Thus, this device is expected to be used in ophthalmic diagnosis in the future.

ERG measurements require a three-electrode system comprising the sensing, reference, and ground electrodes. The sensing electrode is placed in contact with the cornea or conjunctiva, the reference electrode in contact with the ear, and the ground electrode in contact with the tongue. Corneal sensing electrodes typically consist of a rigid contact lens with a metal conductor around the edge to avoid blocking light, whereas conjunctival sensing electrodes are placed on the conjunctiva and are made of a metal conductor in the shape of a ring, hook, or wire.<sup>[6]</sup> Owing to the placement of the corneal sensing electrode, the amplitude of the signal obtained was higher than that from a conjunctival electrode.<sup>[7,8]</sup> However, direct contact between a rigid contact lens and the soft and sensitive eye can cause discomfort during measurements. To overcome this issue,

## 1. Introduction

Electroretinography (ERG) measures the changes in the electrical potential generated by various types of retinal neurons and non-neuronal cells on the corneal surface in response to light stimulation.<sup>[1]</sup> Unlike capturing pictures<sup>[2]</sup> and 3D scanning, this method involves measuring corneal potential changes to diagnose or detect various eye diseases, such as glaucoma, retinitis pigmentosa, diabetic retinopathy, retinal detachment/splitting, and other congenital degenerations.<sup>[3–5]</sup>

flexible and optically transparent electrodes have been developed for soft contact lenses, providing higher signal amplitudes and greater patient comfort.<sup>[9]</sup>

Several types of ERG measurements are currently available, including full-field electroretinograms (FF-ERG), multifocal electroretinograms (MF-ERG), and multi-electrode electroretinograms (ME-ERG). FF-ERG measures the ERG response from the entire corneal surface and requires a single electrode and light stimulation of the entire corneal area. However, the spatial differences in the ERG responses across the cornea cannot be investigated. In contrast, MF-ERG and ME-ERG can be used to study the spatial distribution of corneal responses. MF-ERG requires a single electrode and a high-resolution light stimulator to focus on specific small areas of the cornea.<sup>[10,11]</sup> In contrast, ME-ERG uses multiple electrodes distributed across different areas of the cornea, requiring light stimulation of the whole corneal area; therefore, the spatial resolution requirements of the optical stimulator are not high,<sup>[10,12]</sup> thus rendering it an ideal choice for a flexible and transparent ERG measurement device. The measurement of ME-ERG requires the insulation of the connecting wire from the surface of the cornea so that the sensing region can accurately measure the ERG signal of a specific position on the eye without electrical interference from other points of the cornea caused by the retina's electrical activity. In the past, measurements based on soft contact lenses were mainly used for single-electrode measurements of FF-ERG and MF-ERG<sup>[13,14]</sup>, while

L. Hu, S. Azhari, Q. Li, H. Zhang, T. Miyake  
Graduate School of Information, Production and Systems  
Waseda University  
2-7 Hibikino, Wakamatsu, Kitakyushu, Fukuoka 808-0135, Japan  
E-mail: [miyake@waseda.jp](mailto:miyake@waseda.jp)  
A. Ashimori, K. Kimura  
Department of Ophthalmology  
Yamaguchi Univ.  
1-1 Minami-Kogushi 1-chome, Ube-shi, Yamaguchi 755-8505, Japan  
T. Miyake  
PRESTO  
Japan Science and Technology Agency  
4-1-8 Honcho, Kawaguchi, Saitama 332-0012, Japan

 The ORCID identification number(s) for the author(s) of this article can be found under <https://doi.org/10.1002/admt.202400075>

DOI: 10.1002/admt.202400075

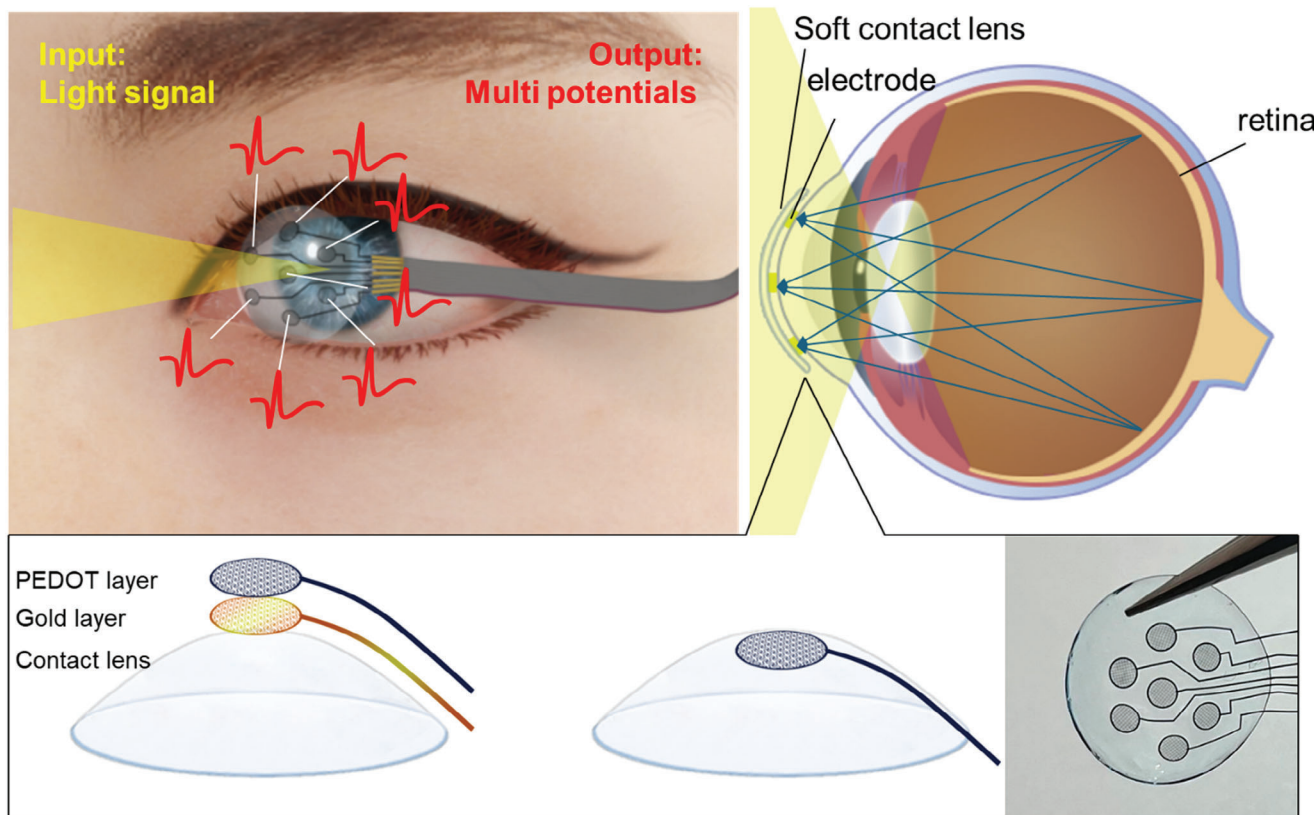


**Figure 1.** Illustration of multi-electrode-electroretinogram (ME-ERG) recording in response to a light stimulus from a human eye using the microelectrode array. Illustration of measurement and device fabrication mechanism and image of the fabricated device.

ME-ERG measurements were mostly performed using hard contact lenses.<sup>[15]</sup> Although there are other reports regarding the use of multielectrode arrays to perform ERG measurement, to our knowledge, none so far have successfully attached their electrode system to soft commercially available contact lenses and insulated the electrodes while keeping the sensing region active.<sup>[16]</sup> ME-ERG measurements were mostly made with hard contact lenses using materials such as SU-8 as the insulating layer. In order to realize a practical ME-ERG system built on commercially available disposable soft contact lenses, we adopted a novel approach to tackle this issue.

Here, we aimed to develop a soft, transparent, multi-electrode system assembled on commercially available soft contact lenses and assess its application in measuring ERG responses in rabbits (Figure 1a). The PEDOT layer is overoxidized to generate a highly resistive (HR) layer on the connecting wire of the multi-electrode system made of gold using DC voltage while keeping the highly conductive sensing region unaltered.<sup>[17]</sup> Gold was used as the electrode material due to its high conductivity, malleability, and biocompatibility. Moreover, using commercially available soft contact lenses as the basis for this system enables adaptability and a close interface with the cornea, resulting in higher signal amplitudes in the measured ERG responses than in rigid contact lens electrodes.<sup>[9]</sup> The distribution of electrodes in different areas of the cornea also enables the investigation of spatial differences in ERG responses, which can be advantageous in the diagnosis and early detection of diseases affecting specific regions of the

eye, such as localized blind spots associated with glaucoma or retinitis pigmentosa.

## 2. Results and Discussion

### 2.1. Preparation of a Multi-Electrode System

The microelectrode array consisted of serpentine mesh electrodes strategically positioned on the inner surface of a disposable soft contact lens close to the corneal surface. To ensure secure attachment of the electrodes to the soft contact lens, a conductive and biocompatible polymer, poly(3,4-ethylenedioxythiophene) (PEDOT), was electrochemically polymerized around the entire outer surface of the microelectrodes, forming a thin encapsulating layer. The mesh electrodes were connected to the copper wires using Ag paste, and a layer of insulating epoxy resin was used to prevent electrical interference (Figure S1, Supporting Information).<sup>[18,19]</sup>

Figure S2 (Supporting Information) shows a schematic illustration of the serpentine mesh electrode used as the microelectrode array. A micropattern of the mesh electrode on the indium tin oxide (ITO) substrate was fabricated using photolithography and electroplating. Briefly, LOR10A was spin-coated on an ITO glass substrate before the photoresist, S1818G, followed by light exposure and substrate immersion in the developer solution (MF319). Gold was electrochemically deposited onto a patterned ITO substrate using a gold plating solution. Finally, the patterned

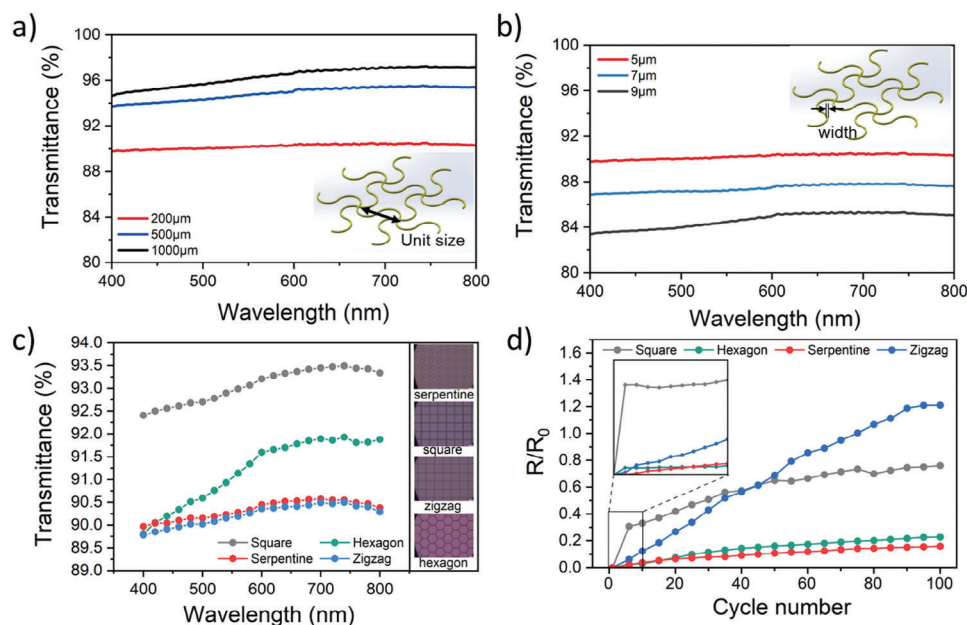


**Figure 2.** Design structure and optical and mechanical properties of electrodes. a) Transmittance of electrodes of different widths. b) Transmittance of electrodes of different unit sizes. c) The transmittance of electrodes with different patterns. d) Strain (10%) test of different electrode patterns for 100 cycles.

gold was peeled off from the ITO substrate in an aqueous solution using tweezers.

After obtaining the serpentine mesh electrodes, we used an electrochemical bonding method to bond the electrodes to the soft contact lenses (Figure S3a, Supporting Information).<sup>[20]</sup> Before the 3,4-ethylenedioxythiophene (EDOT) polymerization, we immersed the contact lens in an electrolyte solution containing  $50 \times 10^{-3}$  M of the EDOT monomer and  $100 \times 10^{-3}$  M of the  $\text{LiClO}_4$  dopant. After the mesh electrode was positioned on the monomer-containing lens, an electrochemical potential of 1.0 V versus Ag/AgCl was applied to the mesh electrode to polymerize EDOT (Figure S3b, Supporting Information). During polymerization, we observed a change in color from the gold of the mesh electrode to the dark blue of the PEDOT/mesh electrode (Figure S3c, Supporting Information). PEDOT was polymerized onto the gold electrode while adhering to the lens. Considering that electrochemical bonding may affect the light transmittance of the mesh electrode, we measured the light transmittance of the mesh electrode before and after bonding and found that it decreased by  $\approx 7\%$  and was still more than 80% (Figure S3d, Supporting Information). Therefore, the electrochemical bonding did not exhibit a significant effect on the light transmittance of the mesh electrode.

## 2.2. Optical and Mechanical Characterization of the Mesh Electrode

ERG is used to measure changes in the electric potential at the corneal surface in response to light stimuli. The corneal electrode must have high transmittance to ensure accurate data collection. In addition, the contact lens may be slightly deformed as the intraocular pressure changes constantly. Therefore, the depen-

dence of the transmittance and deformation of the metal mesh electrodes on parameters such as the width, unit size, and pattern shape of the gold mesh was evaluated.

Figure 2a shows the effect of varying the mesh width while keeping the unit size constant at 200 μm. The transmittance values for widths of 5, 7, and 9 μm were determined to be 90.2%, 87%, and 85%, respectively. Moreover, as shown in Figure 2b, three-unit sizes of 200, 500, and 1000 μm were tested while maintaining a constant width of 5 μm. The transmittance values for the unit sizes of 200, 500, and 1000 μm were found to be 90.2%, 95.3%, and 97.1%, respectively. These findings suggested that an increase in the mesh width decreased transmittance, whereas an increase in unit size increased transmittance.

Based on these results, we concluded that small width and large unit size are required to obtain high transmittance. However, as the diameter of the fabricated circular electrodes is 2 mm, the use of a mesh with a 1000 μm unit size is impractical. The use of large unit sizes increases the sparsity, resulting in the fragility of the electrodes. Therefore, to ensure more than 90% transmittance, the final values for the width and unit size of the mesh electrodes were set at 5 and 200 μm, respectively.

Furthermore, we designed four mesh patterns: square, zigzag, serpentine, and hexagonal (Figure 2c). Similarly, the transmittance of these patterns using a mesh with a unit size of 200 μm and width of 5 μm was investigated. Figure S4 (Supporting Information) displays the details of the serpentine and zigzag pattern design. The transmittances of the square, hexagon, serpentine, and zigzag patterns were 93.2%, 92.1%, 90.2%, and 90.3%, respectively. Notably, the transmittance values for all four patterns were similar and exceeded 90%, indicating relatively high transmittance.

To investigate the optical and mechanical properties of the mesh electrodes, the sheet resistance variations of the four

patterns (square, zigzag, serpentine, and hexagonal) under cyclic strain were compared, as shown in Figure 2d. We repeated the stretch and release process for up to 100 cycles with a maximum of 10% strain and characterized the sheet resistance of the electrodes after each cycle. Under cyclic strain, the zigzag and square gold-mesh electrodes exhibited faster, and more severe resistance increases than the serpentine and hexagonal electrodes. The hexagonal gold mesh electrode exhibited the best sheet resistance stability after 100 cycles of strain testing. To understand the reason for these observations, the topology of the gold mesh electrodes after cyclic loading was investigated, and the results are shown in Figures S5 and S6 (Supporting Information). A strong correlation between the crack density and sheet resistance was observed. In the cyclic strain tests, fatigue was the primary reason for failure that decreased the conductivity of the mesh electrode. A material's fatigue refers to progressive failure under repeated loadings when the initial loading is insufficient to cause immediate failure. The fatigue life mainly depended on the amplitude of the plastic deformation in each loading cycle.<sup>[21]</sup> Nucleated fractures occurred earlier at positions with significant plastic strain than at those with minor plastic strain. During the first few loading cycles, the fracture was more severe in the square- and hexagonal-mesh electrodes. However, after the initial fractures are formed in the mesh, the broken lines can slide and create significant gaps in subsequent stretching, which helps to mitigate the stress caused by the deformation of the lattice in the surrounding area and prolongs the fatigue life. Therefore, after the first cycle, the resistances of the square and hexagonal electrodes increased remarkably, and the subsequent increase in resistance during successive cycles was relatively slow. The zigzag and serpentine electrodes are subjected to a more localized plastic strain. However, the deformation process of the serpentine mesh was more evenly distributed than that of the zigzag mesh, indicating that the serpentine mesh could absorb some stress during unfolding, resulting in fewer cracks. Therefore, the change in resistance of the serpentine mesh was lesser than that of the zigzag mesh.

Overall, our findings indicated that the mesh design with a unit size of 200  $\mu\text{m}$  and width of 5  $\mu\text{m}$  was optimal for achieving high transmittance in the ERG measurement. At the same time, the choice of pattern among square, zigzag, serpentine, and hexagon did not significantly impact the transmittance, as all patterns exhibited similar values exceeding 90%. However, the transmittance and stretching test results indicated that hexagonal or serpentine mesh electrodes should be preferred.

### 2.3. Conductance Dampening of Wire Connection in the Microelectrode Array

In the case of a microelectrode array, the mesh electrode is the essential component for testing the ERG signals, whereas the wire connection requires insulation. Local ERG signals may change because of certain eye conditions. When the connecting wires are insulated, and the mesh electrodes are used to measure ERG signals, the ME-ERG signals can be analyzed to identify changes in the signals, thus pinpointing the region that defines the pathological changes. Traditionally, an insulating layer such as SU8 has been used to cover wire connections<sup>[13]</sup>, however, this approach

poses challenges for contact lenses because it hinders water and oxygen permeation.

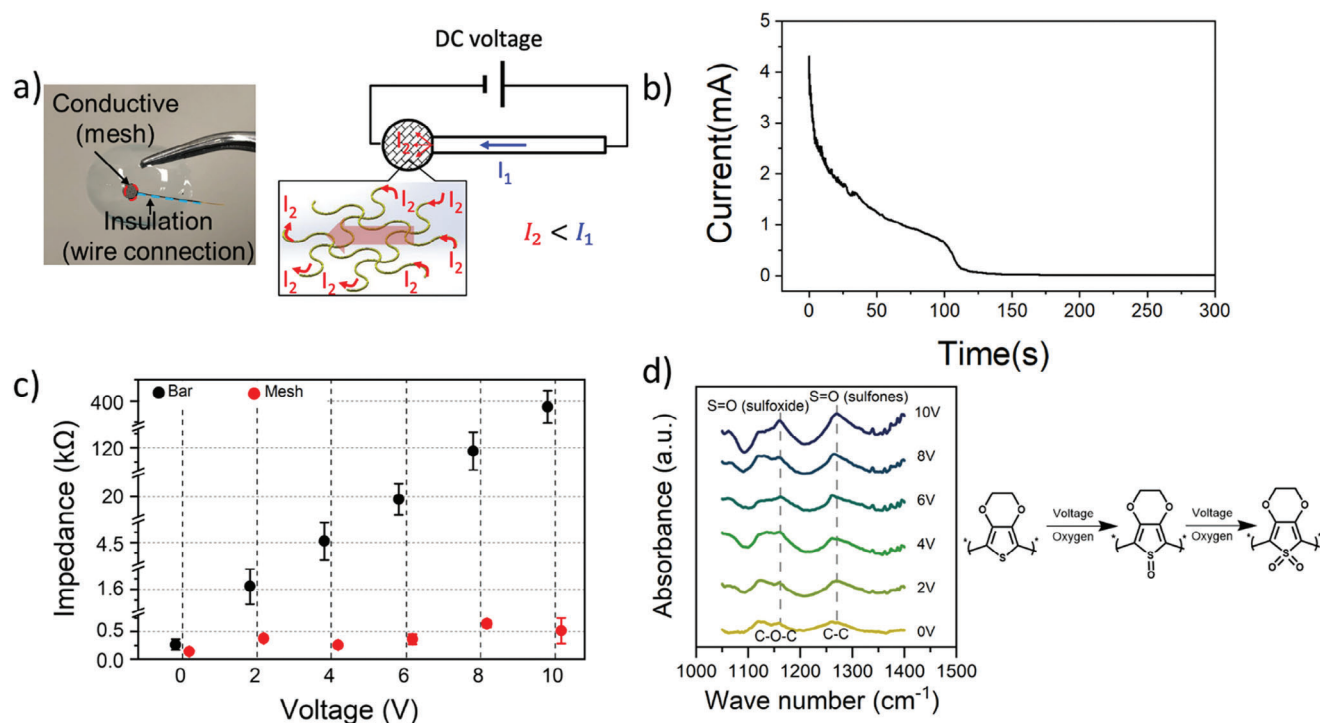
Electrochemical polymerization was used to resolve the insulation issue while maintaining permeation by directly applying a voltage to the microelectrode array in the EDOT solution. This approach significantly increased the impedance of the connecting wire and effectively isolated it while the mesh retained its conductivity (Figure 3a).

Figure 3b provides further insights, showing that when an electrical potential of 10 V is applied for 5 min, the current decreases from 5 mA to 4.5  $\mu\text{A}$ , indicating an increase in resistance. The current reduces substantially immediately upon applying the voltage, reaching a plateau within the first 150 s, and then gradually decreases until the 300 s mark. Based on these observations, a 10 V electric potential was applied to the electrode for 5 min. This approach generates an HR layer on the connecting wire while leaving the mesh undisturbed to measure the ERG signal effectively.

Figure 3c illustrates the change in the current when a DC voltage was applied to the microelectrode array. The impedance was measured at 100 Hz for the connecting wire and mesh electrode after applying DC voltages of 2, 4, 6, 8, and 10 V for 5 min. Initially, the connecting wire exhibited an impedance of  $262.3 \Omega \pm 82.1 \Omega$ . However, upon applying 2, 4, 6, 8, and 10 V, the impedances increased to  $1.65 \text{ k}\Omega \pm 277.23 \Omega$ ,  $4.6 \text{ k}\Omega \pm 1.1 \text{ k}\Omega$ ,  $18.7 \text{ k}\Omega \pm 6.05 \text{ k}\Omega$ ,  $113 \text{ k}\Omega \pm 32.55 \text{ k}\Omega$ , and  $346 \text{ k}\Omega \pm 125.25 \text{ k}\Omega$ , respectively. In contrast, the mesh exhibited an initial impedance of  $141.6 \Omega \pm 23.44 \Omega$ , and upon application of 2, 4, 6, 8, and 10 V, the impedance changed to  $380 \Omega \pm 4.1 \Omega$ ,  $259 \Omega \pm 7.55 \Omega$ ,  $365 \Omega \pm 71.21 \Omega$ ,  $649 \Omega \pm 51 \Omega$ , and  $522 \Omega \pm 190.74 \Omega$ , respectively. These results demonstrated that the impedance of the connecting wire changed significantly as the applied voltage increased, surpassing a 1000-fold increase at 10 V, whereas the mesh exhibited only a slight increase in impedance.

The electrical properties of the connecting wire were affected by the direct current, while the impedance of the mesh remained relatively unchanged. This is attributed to the higher current flowing through the connecting wire, which leads to an overoxidative reaction in the PEDOT layer in the presence of air and an increase in impedance. However, a small amount of current flows through the mesh owing to current division, which prevents a significant overoxidative reaction and maintains a relatively low impedance.

We used the COMSOL Multiphysics simulation to verify the difference between the current in the connection wire ( $I_1$ ) and the current in the mesh part ( $I_2$ ), and to study the influence of different mesh patterns on the difference in current ratio ( $I_1 / I_2$ ). Figure S7 (Supporting Information) shows different designs and orientations of the simulated electrodes. In the design with partial connecting wires, the current density along the horizontal mesh centerline was  $52.3 \text{ A mm}^{-2}$ . For the circular connecting wire (Figure S7b, Supporting Information), the current density along the horizontal mesh centerline was  $33.1 \text{ A mm}^{-2}$ . The current was concentrated in the central region of the partially connected wire, whereas the circularly connected wire exhibited a more evenly distributed current density across the entire mesh. However, it is noteworthy that in the entirely covered circular connecting wire, the current density along the vertical mesh centerline was  $2.19 \times 10^{-4} \text{ A mm}^{-2}$ , indicating higher current density in the



**Figure 3.** Selective isolation using PEDOT. a) The isolated electrode was attached to the soft contact lens via electro-polymerization. b) Variation of current with time during overoxidation. c) Impedance (100 Hz) of the wire connection (bar) and mesh part under different applied voltages. d) FTIR data of connecting wire with the applied electric potentials of 0, 2, 4, 6, 8, and 10 V. Error bars represent the SD of three parallel measurements. Data are presented as the mean  $\pm$  SD ( $n = 3$ ).

direction parallel to the bar outside the mesh and lower current density in the vertical direction.

The direction of the connecting wire was changed to  $45^\circ$  (Figure S7c, Supporting Information) to achieve a more uniform current distribution within the mesh area. After rotating the bar, the current density along the vertical and horizontal mesh centerlines became  $23.8 \text{ A mm}^{-2}$ , which was lower than the previous  $33.1 \text{ A mm}^{-2}$ . Hence, a completely covered pattern with a connecting wire at an angle of  $45^\circ$  was selected.

Furthermore, we investigated the influence of different mesh patterns, including square, serpentine, zigzag, and hexagon, on the ratio of current  $I_1$  over  $I_2$  (denoted as “a” in Figure S8, Supporting Information).  $I_1$  is the product of the current density and cross-sectional area of the connecting wire, whereas  $I_2$  is the average current density multiplied by the cross-sectional area of the mesh part. The cross-sectional area of the connecting wire was 20 times that of the mesh. The values for the square, serpentine, zigzag, and hexagonal patterns were 54.3, 79.4, 68.7, and 61.5, respectively. The value for the serpentine pattern was the highest, followed by those of the zigzag and hexagonal patterns, with the square pattern exhibiting the lowest value. This difference can be attributed to the length of the serpentine pattern, which was the greatest, followed by that of the zigzag and hexagonal patterns, which were more significant than that of the square pattern. This can be explained by the equation,  $R = \rho \frac{l}{A}$ , where  $R$  is resistance,  $\rho$  is the resistivity of the material,  $l$  is length, and  $A$  is the cross-sectional area. The resistance increased with the length of the wire in the mesh patterns, resulting in a reduction in  $I_2$  and an

increase in the  $I_1/I_2$  ratio. Therefore, the serpentine pattern was the most favored choice.

Figure 3d shows the Fourier transform-infrared (FTIR) spectra of the connecting wires with applied electric potentials of 0, 2, 4, 6, 8, and 10 V. The deep blue curve represents the FTIR data of the sample with an applied electric potential of 0 V. The two peaks observed at  $1150$  and  $1280 \text{ cm}^{-1}$  corresponded to C—O—C stretching and C—C stretching vibrations, respectively.<sup>[22]</sup> After applying the DC voltage, the peaks became stronger as their steepness increased with voltage. This increase in peak strength indicated the occurrence of overoxidation in the PEDOT layer. In particular, overlap was observed between the C—O—C stretching and the S=O stretching (sulfoxide) peaks, and the C—C stretching and the S=O stretching (sulfones) peaks.<sup>[23]</sup> The FTIR data in Figure 3d also illustrate the progressive formation of sulfone and sulfoxide structures in the thiophene ring during overoxidation.<sup>[17]</sup> During this overoxidative process, the formation of sulfone and sulfoxide structures gradually increases, leading to a decrease in the conductivity of PEDOT and an increase in impedance.<sup>[24]</sup> The minimal change in the impedance observed in the mesh was attributed to the distribution of the current among the mesh lines, resulting in a small localized current that was not sufficient to induce any overoxidative reaction. In conclusion, based on the results obtained, the design comprising of the entirely covered circular connecting wire, with the wire connection at  $45^\circ$  angle, and a serpentine pattern with unit size of  $200 \mu\text{m}$  and width of  $5 \mu\text{m}$ , were selected for the electrode.

Next, the performance of the HR and conductive electrodes on the contact lenses was tested. A voltage divider circuit with a

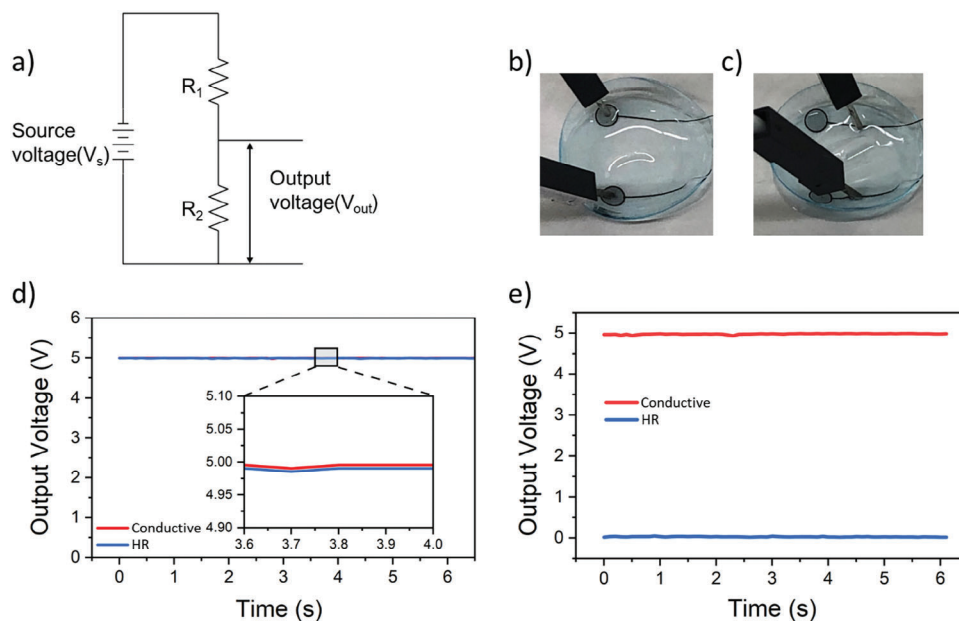


**Figure 4.** Conduction of HR and conductive electrodes on contact lenses. a) Schematic showing the test circuit. b) Photograph of simultaneous conduction test for HR and conductive mesh and c) wire connection. d) The HR and conductive electrodes mesh output voltage measured simultaneously. e) The HR and conductive electrodes wire connection output voltage measured simultaneously.

source voltage of 5 V was used, where resistor  $R_1$  represented the electrode on the contact lens, and resistor  $R_2$  had a fixed value of  $1000 \Omega$ , while the voltage drop across  $R_2$  was measured (Figure 4a). Figure 4b shows the simultaneous measurements of both the HR and conductive meshes and the connecting wire parts. Figure 4c depicts the voltage division when simultaneously measuring the HR and conductive mesh sections. We observed that when measuring the mesh sections, whether HR or conductive, the voltage across  $R_2$  remained consistently above 4.8 V, while the resistance of  $R_1$  remained below  $40 \Omega$ . This indicated that both the HR and conductive mesh sections exhibited high conductivities. Figure 4d shows the simultaneous measurements of the HR and conductive wire connections. When measuring the HR wire connection, the voltage drop across  $R_2$  was only  $\approx 0.02$  V, whereas it remained above 4.8 V when measuring the conductive wire connection. Consequently, we deduced that the resistance of the HR wire connection was above  $200 \text{ k}\Omega$ , while the resistance of the conductive wire connection was relatively low. In summary, the mesh parts of both the HR and conductive electrodes exhibited high conductivity. However, only the HR wire connection demonstrated significantly higher resistance.

## 2.4. Biocompatibility and ERG Testing

To investigate the performance of a fabricated device in living beings, the biocompatibility of the device has to be confirmed. Analysis of the time-dependent cytotoxicity of the microelectrode arrays in human corneal cell lines is important for identifying adverse reactions in vitro. Figure S9a (Supporting Information) shows the viability assay of human corneal cells (HCE) that were seeded on the surface of an Au microelectrode array, Au microelectrode array with a PEDOT layer, and that with a

Zn layer in a culture medium at  $37^\circ\text{C}$ . The cell viability was  $95.5\% \pm 1.22\%$  and  $95\% \pm 1.41\%$  at the end of 72 h assay period for Au and Au covered with a PEDOT layer, respectively, while it was  $30.83\% \pm 6.9\%$  for Au covered with the Zn layer at the end of the entire assay period (72 h). In addition, pictures of the electrode with the original cells, calcein AM-treated cells, and propidium iodide-treated cells are shown in Figure S9b (Supporting Information). Most cells were alive for the Au and PEDOT electrodes, whereas most cells were dead for the Zn electrode. These results indicated that gold and PEDOT are not biotoxic, whereas Zn exhibits biotoxicity owing to its reaction with water, which leads to necrobiosis. This also showed that the microelectrode array is associated with negligible risk of corneal inflammation during ERG examination.

Figure 5a depicts the seven-electrode serpentine mesh used for the ME-ERG measurements. Figure 5b shows the ERG recording process for the rabbit eyes using a Ganzfeld stimulator (RETI port/scan 21, Roland Consult). This stimulator generated a series of short-wavelength stimuli under low-intensity light. We compared the measurements of the ERG signals using a serpentine mesh electrode and a conventional rod electrode (Figure 5c). The amplitude of the ERG signal recorded using the serpentine mesh electrode was  $165 \mu\text{V}$ , which was more than the  $156 \mu\text{V}$  observed with the rod electrode. These results suggested that the flexibility and optical transparency of the serpentine mesh electrodes resulted in a more robust signal.

For the ME-ERG measurement, the electrodes were positioned on the rabbit eye, as shown in Figure 6a, and the response waveforms from different channels under stimulation intensity of  $0.3 \text{ cd s m}^{-2}$  were recorded (Figure 6b). Each channel detected a typical ERG signal with characteristic a- and b-waves,<sup>[25]</sup> similar to the conventional single-electrode FF-ERG recording. The amplitudes decreased with increasing distance from the corneal

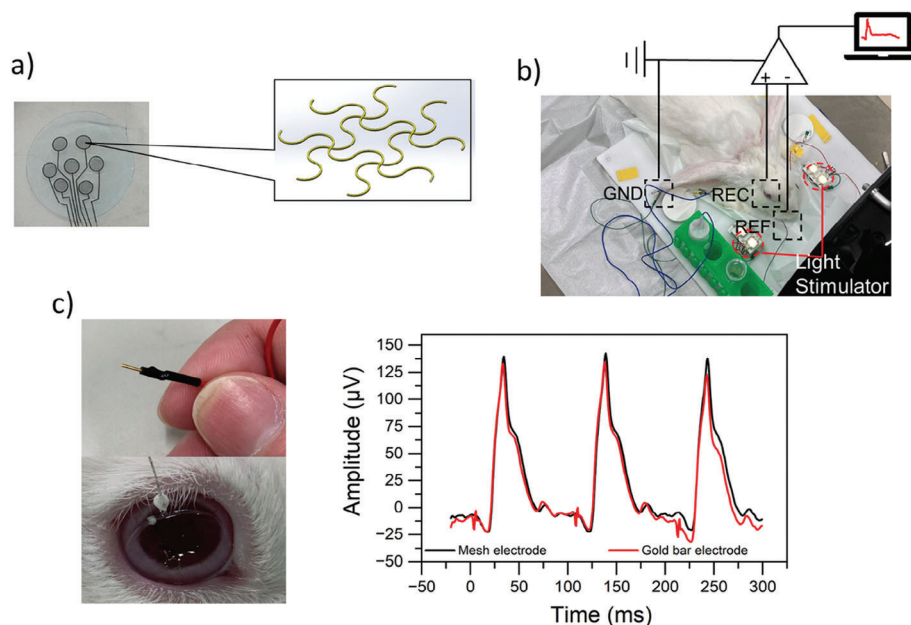


**Figure 5.** ME-ERG testing. a) Photograph of seven microelectrode array. b) ERG test setup on rabbit eyes. c) Representative ERG signals recorded using our electrode and a gold bar electrode from the same eye of a rabbit.

center, indicating that the amplitudes were higher in the central cornea than at the periphery. This variation may reflect the intrinsic spatial differences in the ERG potential across the cornea, as previously observed and reported by other groups.<sup>[13,15]</sup> This showed that a soft and transparent multi-electrode array can effectively measure the terrain of corneal ERG potentials. This analogy was further tested by collecting the output from each electrode sixteen times under the same stimuli. As shown in Figure S10 (Supporting Information), the amplitude of the collected

ERG signals varied depending on the electrode position, with the maximum in electrode number 4 ( $180.85 \mu\text{V} \pm 11.35 \mu\text{V}$ ), which was significantly higher than all other electrodes ( $p < 0.001$ ).

### 3. Conclusion

We introduced the fabrication of a transparent and flexible multi-electrode system on commercially available soft contact lenses. The effectiveness of the fabricated device in recording the

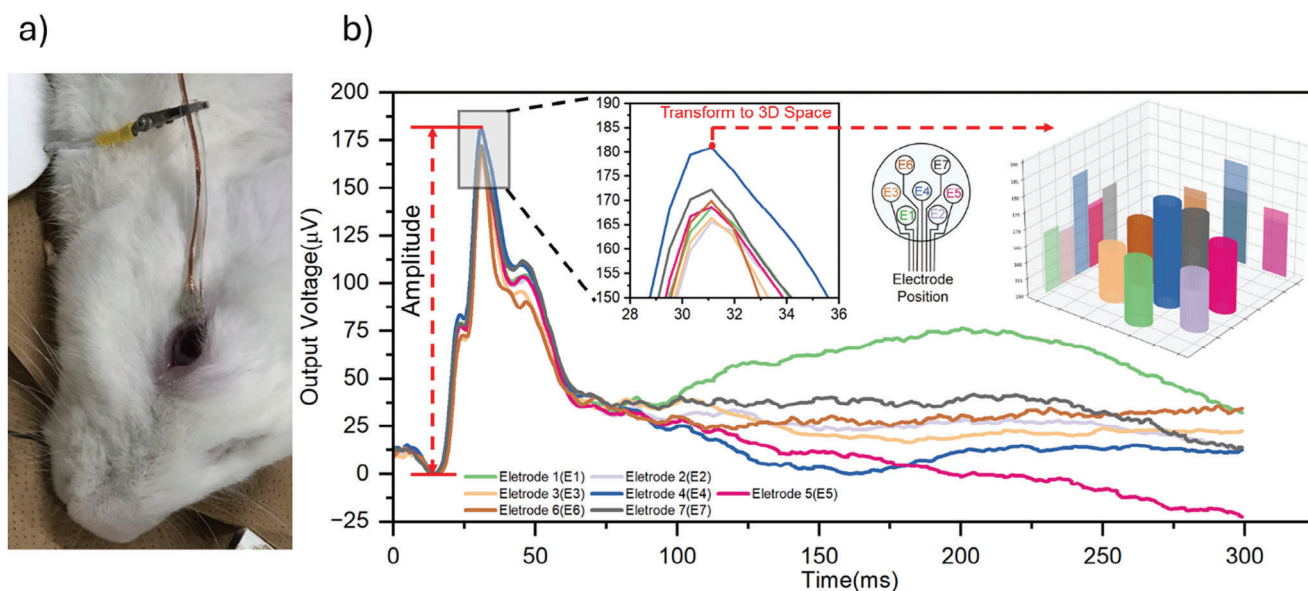


**Figure 6.** ME-ERG recording. a) A multi-electrode positioned over a dilated rabbit eye. b) A representative set of the multi-electrode ERG response waveforms. Stimulus strength,  $0.3 \text{ cd s m}^{-2}$ .

ME-ERG responses of rabbit eyes was demonstrated. The PEDOT layer on the connecting wires of this multi-electrode system was overoxidized using DC voltage, generating an HR layer while the high conductivity in the meshed sensing part was maintained; hence, the need for additional insulation layers was eliminated. This innovative approach provides several advantages over previously developed microelectrodes, including higher biocompatibility, flexibility, oxygen permeability, transparency, and wetability. The ME-ERG recordings in rabbits showed that the ERG signals were higher in the central region than at the periphery. This provides an opportunity to investigate the spatial variations in ERG responses, which can help diagnose and detect diseases affecting specific eye regions. We anticipate that integrating optically transparent and electrochemically bonded flexible electrodes with soft contact lenses and using specialized conductance-dampening techniques will be pivotal in advancing visual electrophysiology research in vivo.

#### 4. Experimental Section

**Fabrication of the Microelectrode Array:** A 2.5 × 2.5 cm ITO substrate (Zhuhai Kaivo Optoelectronic Technology Co., Ltd. China) was washed with acetone, isopropyl alcohol, and deionized water for 5 min each in an ultrasonic bath. A photoresist (LOR10A, Nippon Kayaku Co., Ltd., Japan) was coated on the ITO substrate using a spin coater at 500 rpm for 5 s and at 3,000 rpm for 45 s. The film was heated on a hot plate at 180 °C for 5 min. The second photoresist (S1818G, Nippon Kayaku Co. Ltd., Japan) was coated onto the substrate using a spin coater at 4,000 rpm for 20 s and stabilized by heating on a hot plate at 90 °C for 5 min. The micropattern was fabricated using photolithography (M-2L, Mikasa Co. Ltd., Japan), followed by immersion of the substrate into the developer solution (MF-319, Nippon Kayaku Co. Ltd., Japan). The patterned resist on the ITO substrate was heated on a hot plate at 130 °C for 5 min. Gold was deposited electrochemically on the patterned ITO substrate in a gold plating solution (K-740, Kojima chemicals co. Ltd., Japan) at 60 °C under a constant current of 0.8 mA applied to the ITO for 20 min. The patterned gold was peeled off the ITO substrate using an aqueous solution.

**Electrochemical Attachment:** A commercially available soft contact lens was immersed in a solution containing EDOT (Sigma-Aldrich) ( $50 \times 10^{-3}$  M) and LiClO<sub>4</sub> (Sigma-Aldrich) ( $100 \times 10^{-3}$  M) overnight at 4 °C. The microelectrode was then mounted on a lens containing the EDOT monomer, which was polymerized using a three-electrode system with Ag/AgCl (BAS Inc. Tokyo, Japan) as the reference electrode and Pt (The Nilaco Corporation. Tokyo, Japan) as the counter electrode. The PEDOT adhesive was electropolymerized at 1 V. After polymerization, the soft contact lens was immersed in deionized water for 30 min and then rinsed with saline solution to remove the unreacted EDOT monomer from the contact lens.

**Evaluation of Biocompatibility:** The device was sterilized using ethanol–Deionized water mixture (70:30 v/v) for 30 min, rinsed with phosphate buffered saline (PBS), and dehydrated using UV irradiation (GL-15 Toshiba Corporation., Japan) for 1 h. The sterilized device was placed in a 24-well plate (Thermo Fisher Scientific., China). HCEs ( $1 \times 10^5$  cells/well) were seeded in a cell medium and subsequently incubated in a humidified incubator maintained at 37 °C with 5% CO<sub>2</sub> for 24, 48, and 72 h. Trypsin (Cell Science & Technology Institute, Inc., Japan) was used to wash the cells, followed by washing twice and resuspending in PBS. Cell staining was performed by adding 50 μL trypan blue staining solution (Gibco by Thermo Fisher Scientific., Japan) to an equal volume of cells, mixing gently, and staining for 3–5 min. A small number of stained cells were counted using a cell-counting board (Bio-Rad Laboratories. Inc., USA) to determine the cell survival rate.

**Finite Element Analysis (FEA):** FEA was conducted using the COMSOL AC/DC package. In the finite element model, a 10 V electrical potential was

applied to both ends of the microelectrode to analyze the magnitude and distribution of the current in the microelectrode. The magnitude and distribution of the current in the microelectrodes with different mesh patterns were compared.

**Measurement of Multi-Electrode ERG Signals:** Rabbit was anesthetized via intramuscular injection of a mixture of 0.15 mg kg<sup>-1</sup> medetomidine hydrochloride (Domitor; Nippon Zenyaku kogyo, Japan), 1 mg kg<sup>-1</sup> midazolam (Dormicum, Maruishi Pharmaceutical, Japan), and 1.5 mg kg<sup>-1</sup> butorphanol tartrate (Betfal, Meiji Animal Health, Japan). Their eyes were dilated completely using phenylephrine hydrochloride (0.5%) and tropicamide (0.5%). The multi-electrode was placed on the fully dilated eye of the rabbit. The reference electrode was placed on the rabbit tongue, and the ground electrode was clipped onto its ear. The LS-100 (MAYO Corporation, Japan) was used to provide white light luminous intensity from 0.01 to 10.0 cd s m<sup>-2</sup>. PuREC (MAYO Corporation, Japan) was used to amplify the signals and record the data. The ERG measurement on the rabbit eye was performed sixteen consecutive times for each electrode to obtain the standard deviation and average for each spatial position. The rabbit experiments were approved by the Animal Ethics Committee of the Yamaguchi University Graduate School of Medicine with approval number 41-003. It was performed in accordance with the ARRIVE guidelines for animal research as well as with the ARVO Statement for the Use of Animals in Ophthalmic and Vision Research.

**Statistical Analysis:** The experimental data were organized using Microsoft Excel and analyzed using Origin 2024 (OriginLab). The data were expressed as mean ± standard deviation (SD) and presented without further preprocessing. The conductance dampening and biocompatibility experiments comprised at least three independent experimental batches performed under identical conditions ( $n \geq 3$ ). The ERG measurement on the rabbit eye was performed at least sixteen consecutive times ( $n \geq 16$ ). For parametric results, statistical analysis was performed by one-way analysis of variance (ANOVA) with a Tukey–Kramer post hoc test of the variance. In all cases, significance levels (*p*-values) were indicated with asterisks, and specific *p*-values were provided in each figure legend (\* $p < 0.05$ , \*\* $p < 0.01$ , \*\*\* $p < 0.001$ ).

**Ethics Approval Statement:** The rabbit experiments were approved by the Animal Ethics Committee of the Yamaguchi University Graduate School of Medicine with approval number 41-003. It was performed in accordance with the ARRIVE guidelines for animal research as well as with the ARVO Statement for the Use of Animals in Ophthalmic and Vision Research.

#### Supporting Information

Supporting Information is available from the Wiley Online Library or from the author.

#### Acknowledgements

This work was supported by the AMED under Grant number (JP23hma322020) and the Canon Foundation. Part of this work was conducted at Kitakyushu Foundation for the Advancement of Industry, Science and Technology, Semiconductor Center, supported by “Nanotechnology Platform Program” of the Ministry of Education, Culture, Sports, Science and Technology (MEXT), Japan.

#### Conflict of Interest

The authors declare no conflict of interest.

#### Data Availability Statement

The data that support the findings of this study are available on request from the corresponding author. The data are not publicly available due to privacy or ethical restrictions.

## Keywords

DC voltage overoxidation, electrochemical bonding, electroretinography testing, microelectrode, soft contact lens

Received: January 17, 2024

Revised: April 10, 2024

Published online: May 6, 2024

- 
- [1] J. R. Heckenlively, G. B. Arden, *Principles and Practice of Clinical Electrophysiology of Vision*, MIT Press, Cambridge, MA **2006**.
- [2] Y. Cui, T. Takamatsu, K. Shimizu, T. Miyake, *Appl. Phys. Express* **2022**, *15*, 027001.
- [3] B. Young, E. Eggenberger, D. Kaufman, *Curr. Opin. Ophthalmol.* **2012**, *23*, 497.
- [4] H. P. Scholl, E. Zrenner, *Surv. Ophthalmol.* **2000**, *45*, 29.
- [5] C. Senger, R. Moreto, S. E. Watanabe, A. G. Matos, J. S. Paula, *J. Glaucoma.* **2020**, *29*, 147.
- [6] M. Gjötterberg, *Arch. Ophthalmol.* **1986**, *104*, 569.
- [7] F. Carpi, F. Tomei, *Biomed. Pharmacother.* **2006**, *60*, 375.
- [8] L. Esakowitz, A. Kriss, F. Shawkat, *Eye* **1993**, *7*, 169.
- [9] K. Kim, H. J. Kim, H. Zhang, W. Park, D. Meyer, M. K. Kim, C. H. Lee, *Nat. Commun.* **2021**, *12*, 1544.
- [10] D. C. Hood, M. Bach, M. Brigell, D. Keating, M. Kondo, J. S. Lyons, *Doc. Ophthalmol.* **2012**, *124*, 1.
- [11] N. Mohidin, M. K. Yap, R. J. Jacobs, *Sains Malays* **2014**, *43*, 1089.
- [12] D. C. Hood, J. G. Odel, C. S. Chen, B. J. Winn, *Neuro-Ophthalmol* **2003**, *23*, 225.
- [13] R. Yin, Z. Xu, M. Mei, Z. Chen, K. Wang, Y. Liu, X. Duan, *Nat. Commun.* **2018**, *9*, 2334.
- [14] S. Wei, R. Yin, T. Tang, Y. Wu, Y. Liu, P. Wang, K. Wang, M. Mei, R. Zou, X. Duan, *ACS nano.* **2019**, *13*, 7920.
- [15] Y. Krakova, H. Tajalli, S. Thongpang, Z. Derafshi, T. Ban, S. Rahmani, A. N. Selner, A. A. Tarouti, J. C. Williams, J. R. Hetling, *Doc. Ophthalmol.* **2014**, *129*, 151.
- [16] J. de La Cruz, D. Nguyen, X. Illa, J. Bousquet, A. P. Pérez-Marín, E. del Corro, S. Picaud, J. A. Garrido, C. Hebert, *Adv. Mater. Technol.* **2022**, *7*, 2101181.
- [17] J. Fan, S. S. Rezaie, M. Facchini-Rakovich, D. Gudi, C. Montemagno, M. Gupta, *Org. Electron.* **2019**, *66*, 148.
- [18] Y. Ogawa, K. Kato, T. Miyake, K. Nagamine, T. Ofuji, S. Yoshino, M. Nishizawa, *Adv. Healthcare Mater.* **2015**, *4*, 506.
- [19] H. Kai, T. Yamauchi, Y. Ogawa, A. Tsubota, T. Magome, T. Miyake, K. Yamasaki, M. Nishizawa, *Adv. Healthcare Mater.* **2017**, *6*, 1700465.
- [20] T. Takamatsu, Y. Chen, T. Yoshimasu, M. Nishizawa, T. Miyake, *Adv. Mater. Technol.* **2019**, *4*, 1800671.
- [21] C. Zhang, A. Khan, J. Cai, C. Liang, Y. Liu, J. Deng, W. D. Li, *ACS Appl. Mater. Interfaces.* **2018**, *10*, 21009.
- [22] G. Hassan, M. Sajid, C. Choi, *Sci. Rep.* **2019**, *9*, 15227.
- [23] B. P. Vinayan, Z. Zhao-Karger, T. Diemant, V. S. K. Chakravadhanula, N. I. Schwarzbürger, M. A. Cambaz, M. Fichtner, *Nanoscale* **2016**, *8*, 3296.
- [24] A. J. Oostra, K. H. van den Bos, P. W. Blom, J. J. Michels, *J. Phys. Chem. B.* **2013**, *117*, 10929.
- [25] R. F. Miller, J. E. Dowling, *J. Neurophysiol.* **1970**, *33*, 323.